JACS
JOURNAL OF THE AMERICAN CHEMICAL SOCIETY

Article

pubs.acs.org/JACS

The Reversible Opening of Water Channels in Cytochrome *c* Modulates the Heme Iron Reduction Potential

Carlo Augusto Bortolotti,[†] Andrea Amadei,[‡] Massimiliano Aschi,[§] Marco Borsari,[†] Stefano Corni,[∥] Marco Sola,[†] and Isabella Daidone*[,§]

[†]Department of Life Sciences, University of Modena and Reggio Emilia, Via Campi 183, 41125, Modena, Italy

[‡]Department of Chemical Sciences and Technologies, University of Rome "Tor Vergata", via della Ricerca Scientifica 1, 00133 Rome, Italy

[§]Department of Physical and Chemical Sciences, University of L'Aquila, via Vetoio (Coppito 1), 67010 L'Aquila, Italy

[∥]Centro S3, CNR-NANO Istituto Nanoscienze-CNR, Via Campi 213/A, 41125 Modena, Italy

Supporting Information

ABSTRACT: Dynamic protein−solvent interactions are fundamental for life processes, but their investigation is still experimentally very demanding. Molecular dynamics simulations up to hundreds of nanoseconds can bring to light unexpected events even for extensively studied biomolecules. This paper reports a combined computational/experimental approach that reveals the reversible opening of two distinct fluctuating cavities in *Saccharomyces cerevisiae* iso-1-cytochrome *c*. Both channels allow water access to the heme center. By means of a mixed quantum mechanics/molecular dynamics (QM/MD) theoretical approach, the perturbed matrix method (PMM), that allows to reach long simulation times, changes in the reduction potential of the heme Fe^{3+}/Fe^{2+} couple induced by the opening of each cavity are calculated. Shifts of the reduction potential upon changes in the hydration of the heme propionates are observed. These variations are relatively small but significant and could therefore represent a tool developed by cytochrome *c* for the solvent driven, fine-tuning of its redox functionality.

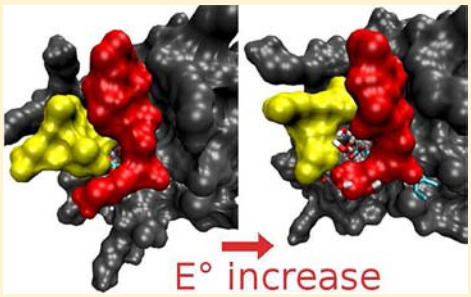

INTRODUCTION

Thermal fluctuations and concerted movements at the molecular level in proteins are essential for fundamental biological processes, such as protein folding, protein−protein recognition, and electron transfer (ET).[1−4] Therefore, protein dynamics are central to the accomplishment of crucial physiological functions.[5,6] It is now widely accepted that proteins cycle over all the allowed higher energy forms, undergoing constant unfolding and refolding processes;[7] nevertheless, most experimental techniques are informative only on the lowest free energy states, since these are highly more populated and therefore dominate the response of the biosystems under investigation. Proteins under native conditions display a much larger structural heterogeneity than that shown in a crystal structure;[8] therefore, investigations that allow a large number of conformational states to be probed and provide time-dependent structural information are essential for a deeper understanding of the structure/function relationships.[8−12] From an experimental point of view, the dynamic properties of proteins can usually be only indirectly inferred by the measurements of physical observables carried out with extremely sophisticated methods.[8] These techniques suffer from low spatial or time resolution that make them scarcely informative at the actual state of the art.[6]

The coupling of experiments and simulation techniques, providing dynamical information at the molecular level, would be the most promising approach to connect structural changes over time to functional properties of a biomolecule. Nevertheless, a reliable modeling of chemical reactions taking place in a protein environment and, in general, in complex systems, is one of the challenges of theoretical chemistry and biophysics.[11,13−17] The primary difficulty is represented by the need of maintaining the electronic detail of the chemical reaction within a configurationally complex atomistic environment. However, an extensive sampling of atomic motion in combination with high-level electronic-structure calculations is still challenging for systems of the required size and complexity. Therefore, simplifying assumptions and/or limited phase space sampling characterize many of the commonly utilized theoretical approaches (see ref 18 and references therein).

We recently developed a mixed quantum mechanics/molecular dynamics (QM/MD) theoretical/computational approach, based on the perturbed matrix method (PMM).[19−22] This method allows for the calculation of electronic properties in complex systems and is not limited in the configurational sampling. Moreover, it does not involve

Received: March 29, 2012
Published: August 9, 2012

   dx.doi.org/10.1021/ja3030356 | J. Am. Chem. Soc. 2012, 134, 13670−13678

empirical/adjustable parameters. A possible drawback of the lack of adjustable parameters is that our methodology might be less accurate than other methodologies in reproducing the absolute values of the observable under investigation. The underlying perspective of PMM, in line with all QM/MM procedures,[23,24] relies on the predefinition of the quantum center (QC), i.e., a portion of the system to be explicitly treated at the electronic level, with the rest of the system described at a classical atomistic level exerting an electrostatic perturbation on the quantum-center electronic states. As the phase space sampling is provided by classical MD, a statistically relevant sampling of the quantum-center/environment configurations can be achieved, which is necessary for a proper description of functional properties in dynamical, complex systems, such as ET processes in proteins, and is commonly not accessible to other computational techniques.

Cytochrome *c* (cyt *c*) is one of the most widely investigated ET proteins. Englander and co-workers described cyt *c* as composed by concerted unfolding units, called "foldons", basically coincident with secondary structure elements (α-helices and Ω loops)[25] (see Figure 1). Recent experimental studies[6,7,25] showed that foldon units undergo constant folding/unfolding processes, even under native conditions, and suggested that local unfolding could be one of the strategies developed to control not only the folding behavior but the overall biological activity of cyt *c*, namely its involvement in apoptosis, the alkaline transition, and most interestingly its redox activity. The peroxidase activity of cyt *c* displayed during apoptosis[26,27] was suggested to be related to the formation of a channel in the protein globule allowing water molecules access to the heme crevice.[28] This hypothesis is in line with previous computational investigations[29] predicting the opening of a channel in cyt *c* providing water access to the heme distal site. Interestingly, water was recently assigned a major role also in docking of cyt *c* to biological partners[30,31] and in mediating interprotein ET coupling pathways.[32,33] As protein−solvent interactions mostly rely on conformational fluctuations, a fully reliable picture of cyt *c* in action requires new dynamic approaches which could add the time dimension to the structure−function paradigm, with a particular focus on the interplay between the solvent and the protein matrix and on the effects of water on the functionality of the protein.[34]

Here, MD simulations of iso-1-cytochrome *c* from *Saccharomyces cerevisiae* were performed for hundreds of nanoseconds, and use was made of the PMM method mentioned above for the calculation of redox properties. In the MD trajectories reversible opening of two cavities in the protein surface was repeatedly observed, each facing one of the heme propionates. Opening and closing of the cavities allow transient water access into the protein matrix and provide direct access of water molecules to the heme propionates. Interestingly, the opening/closing events were found to be related to the concerted movement of foldon units. The existence of these solvent-exposed conformations, and the transient opening of water-accessible cavities over time, could have hardly been inferred by mere analysis of crystal structures and currently available experimental data. By means of PMM calculations on the MD trajectories we then determined the reduction potential of cyt *c* in water. The reliability of the theoretical approach was tested by performing electrochemical measurements on the same protein. Most notably, the PMM/MD procedure was used to investigate the effects of the transient access of water molecules to the propionates on the reduction potential of the protein, thus correlating the observed dynamical−structural processes to changes in functional properties and strengthening the hypothesis that the cooperative Ω loops likely play a role in controlling the biological redox functionality.

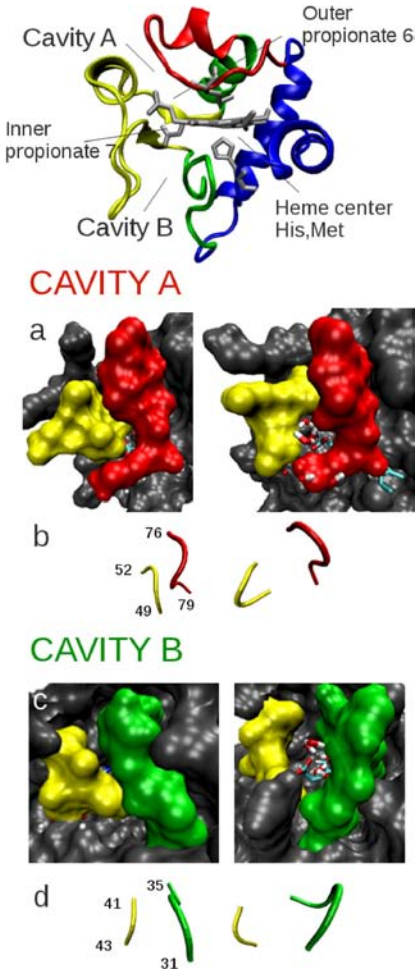

Figure 1. Solvent accessible cavities in cyt *c*. Top: The crystallographic structure of yeast iso-1-cyt *c* (pdb code: 1YCC)[35] features a cluster of three long α-helices, the N-terminal (residues 2−15), the C-terminal (residues 87−102), and the 60s helix (residues 60−69) and three loop regions, namely loops 1 (residues 21−35), 2 (residues 36−59), and 3 (residues 70−85). The 3 helices are grouped around one edge of the heme *c*, which features the two propionates, namely propionate 6 and 7, as substituents of the tetrapyrrole ring. The cartoon representation was created from the crystallographic structure (pdb code: 1YCC),[35] and it is colored according to the collective folding units described by Englander and co-workers.[7,25] The image was produced with the VMD software.[36] (a,c) Representative structures of the closed (left) and open (right) states of cavities A and B, respectively. (b,d) Extreme configurations of the loops involved in opening of cavities A and B, respectively, as obtained by projecting the corresponding C_α coordinates of each MD time frame onto the first essential eigenvector.

In what follows, the reversible opening of solvent accessible channels along the MD trajectories will be described from a structural point of view. We will then focus on the PMM-based calculations of the redox properties of yeast cyt *c* and on their comparison with the experimental values. The last paragraphs of the paper will describe how the functional properties of cyt *c*, in particular its reduction potential, can be affected by the

dx.doi.org/10.1021/ja3030356 | J. Am. Chem. Soc. 2012, 134, 13670−13678

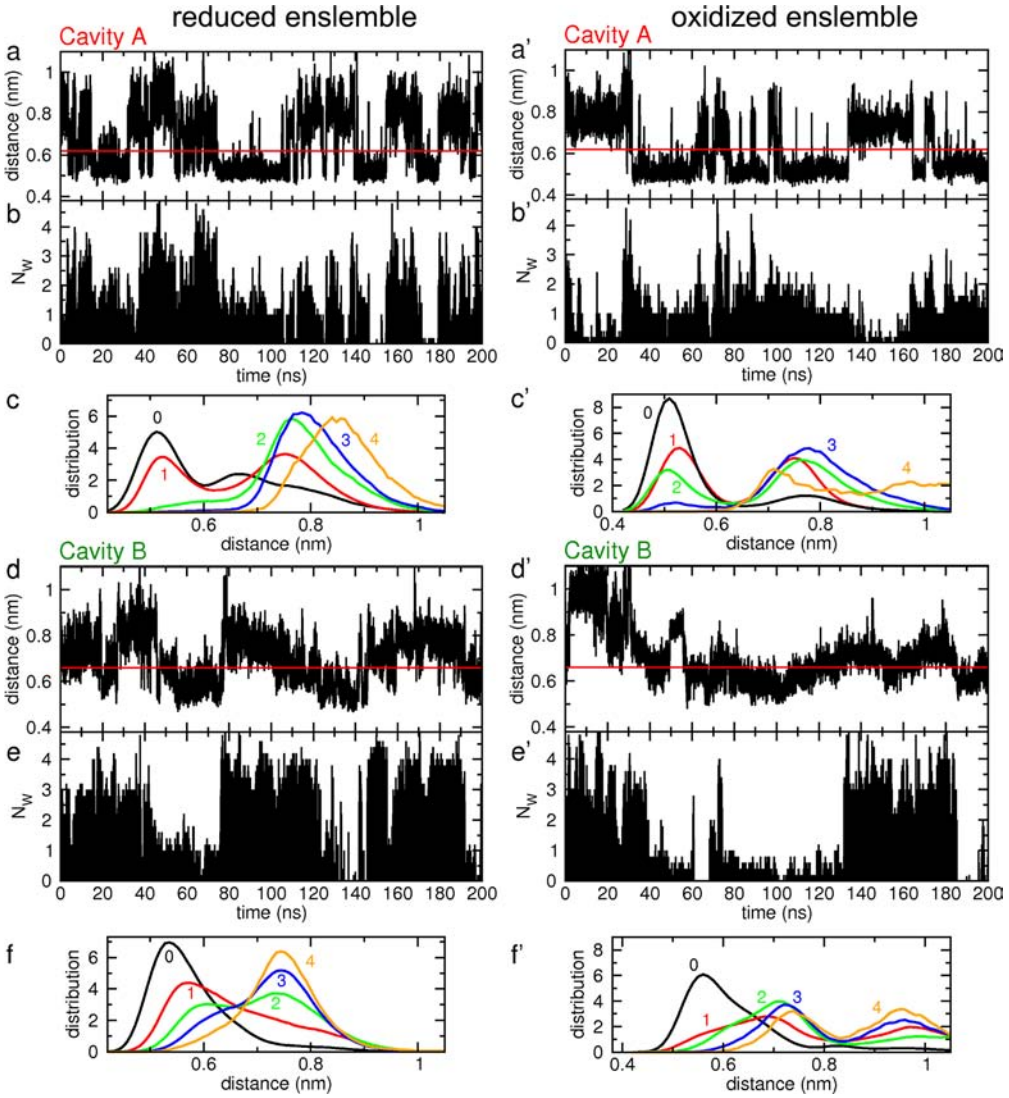

Figure 2. Characterization of the water channels in the reduced (left) and oxidized (right) cyt *c* simulations. (a,a′) and (d,d′) Time evolution of the distance between the C_α atoms of residues 50 and 77 (cavity A, panels a and a′) and residues 31 and 43 (cavity B, panels d and d′) in the MD simulations. The red line highlights the cutoff distance (0.62 and 0.65 nm for cavities A and B, respectively) that was chosen as a reference to discern between closed and open conformations. (b,b′) and (e,e′) Time evolution of the number of water molecules (N_W) inside cavity A (panels b and b′) and cavity B (panels e and e′) in the MD simulations. (c,c′) and (f,f′) Normalized distributions of configurations with a given C_α−C_α distance describing the opening of cavity A (panels c and c′) and cavity B (panels f and f′) calculated by using subpopulations with different numbers of water molecules inside the cavity (0, 1, 2, 3 and ≥4).

presence of water molecules in proximity of the heme propionates.

RESULTS AND DISCUSSION

Structural Behavior of cyt *c* in the MD Simulations. The 200 ns long MD simulations of both reduced and oxidized cyt *c* were performed in aqueous solution (the crystallographic structure of cyt *c* is shown in Figure 1). To test the stability of the simulations, a number of structural parameters were monitored during the time course of each simulation [see Table 1, Supporting Information (SI)]. Their average values were comparable with those calculated from the crystal structures, confirming the stability of the trajectories in time. In particular, analysis of the percentage of helicity of each residue showed that all α-helices are well conserved along the simulations.

Analysis of the Exposure of the Heme Center to the Solvent. The heme center in cyt c is formed by a Fe-protoporphyrin IX covalently attached to the protein matrix through two thioether bonds. Two propionate groups act as ring substituents at positions 6 and 7. Together with the iron axial ligands, His18 and Met80, the heme center is usually considered as the electron-donor/-acceptor group when the problem of the path of the electron during the reduction process is addressed.[37−40] Although the heme center is located inside a hydrophobic pocket, a few ordered water molecules were detected in the crystallographic structures obtained for both iron oxidation states; one, located on the side of the heme displaying the S(Met80)-Fe bond, is considered to be catalytically important. Two more water molecules are located close to the carboxylate group of the inner propionate, (propionate-7), apparently far from the bulk solvent surrounding the protein matrix.[35]

dx.doi.org/10.1021/ja3030356 | J. Am. Chem. Soc. 2012, 134, 13670−13678

The solvent accessibility of the heme center in the simulations was investigated. In both the reduced and oxidized cyt *c* simulations, the formation of two different channels in contact with the bulk solvent could be identified (see Figure 1). Each channel is defined by two groups of residues belonging to loops placed on opposite sides and facing each other. One channel is defined by residues 49−52 on one side and 76−79 on the other (cavity A) and provides direct access to the so-called outer propionate (propionate-6). The other channel (cavity B) is defined by residues 31−35 on one side and 41−43 on the other and allows solvent molecules to enter the protein matrix pointing directly at the inner propionate-7 (see the Methods Section for the determination of the involved residues).

The reversible cavity opening/closing events were related to protein motions by applying the principal component analysis (PCA), or essential dynamics analysis, on the atomic positional fluctuations[41,42] of the residues defining each of the two cavities (see Methods Section for the details). The principal motions associated with the eigenvector with the highest eigenvalue describe, for each cavity, opening/closing movements involving collective motions of the backbone, rather than displacements of single side chains or simple breaking/forming of a hydrogen bond (see Figure 1). One of the most important features of these motions is that they involve the relative displacement of strands of amino acids belonging to Ω loops that were recently proved to act as concerted subunits in folding/unfolding processes:[25] residues 49−52 and 76−79, that define cavity A, belong to the so-called "nested subyellow" (N-yellow) and "red" foldon, respectively.[25] The N-yellow foldon is also involved in the opening/closing of cavity B (through residues 41−43), together with residues 31−35 that belong to the so-called "green" foldon.

The opening and closing of cavity A is well described by plotting the time dependence of the distance between the C_α atoms of residues 50 and 77, lying on opposite sides of the cavity mouth (Figure 2, panels a and a′). The channel is considered open when the distance is higher than 0.62 nm. Similarly, the behavior of cavity B can be investigated by monitoring the distance between the C_α atoms of residues 31 and 43 (Figure 2, panels d and d′), also sitting at opposites sides of the mouth of the channel, which is considered open when the distance between the two C_α atoms is higher than 0.65 nm (the choice of the aforementioned cut-offs was based on the analysis of the probability density; see Methods Section). Opening/closing of the channels allows water molecules to enter and leave the heme crevice, as illustrated in Figure 2, panels b and b′ for cavity A and panels e and e′ for cavity B, in which the time dependence of the number of water molecules inside each cavity is shown for the reduced and oxidized ensembles.

To quantify the correlation between the number of water molecules entering each cavity and the opening/closing motions, the MD structures were clustered according to the number of water molecules residing in each cavity (0−3 and ≥4), and for each cluster the distribution of the C_α−C_α distance defining the opening of the channel was calculated. The results are shown in Figure 2, panels c and c′ for cavity A and panels f and f′ for cavity B. In both cases, three or more water molecules are present in the channel when the cavity is open (i.e., the corresponding C_α−C_α distance is ≥0.62−0.65 nm), while the complete absence of solvent molecules in the channel almost invariably corresponds to a closed conformation (i.e., the corresponding C_α−C_α distance is <0.62−0.65 nm). The cavity opening process appears, thus, to switch at 1−2 water molecules. It should be noted that there is a rather high probability that one or two water molecules can be retained inside the heme crevice when the cavity is closed. However, the crowded environment, the averaging over water occupancy, and the low temperature of the crystal structure prevent a direct comparison with the X-ray data. In conclusion, for both cavities A and B the opening of the channel is accompanied by the access of water to the heme crevice in both the reduced and oxidized ensembles.

Our findings concerning the formation of solvent accessible channels in cyt *c* are supported by hydrogen-exchange experiments performed on cyt *c* at equilibrium native conditions, which revealed that Ω loops undergo transient, reversible unfolding steps;[25] the least stable and fastest unfolding unit in cyt *c* was identified as the segment spanning residues 40−57, which was defined as the N-yellow foldon and is involved in both cavities described in the present work. Moreover, proteolysis studies on cyt *c* showed that the N-yellow loop region is the first to be cleaved by proteases[43,44] because of its higher propensity to transient unfolding. All these data indicate that the N-yellow foldon is the most flexible and prone to partial unfolding under native conditions. Further evidence supporting the formation of the cavities identified here arises from the analysis of the NMR-derived structures of yeast iso-1-ferrocytochrome *c*,[45] which shows that the residues involved in the formation of both cavities described here are among those displaying the highest root-mean-square fluctuation. The observation of transient opening of water-accessible cavities is also supported by the recent discovery of the catalytic activity displayed by cytochrome *c* during apoptosis.[27] In fact, the release of proapoptotic factors was suggested to be related to the formation of a water accessible channel in the protein globule, facilitating the access of H_2O_2 to the heme and thus initiating the peroxidase activity.[27,28] Our findings are consistent with this experimental evidence and further provide insight at a molecular level on the possible mechanisms through which hydrogen peroxide molecules have access to the heme crevice.

Thermodynamic Properties of the Fe^{3+}→Fe^{2+} Process. Cyclic voltammetry (CV) experiments were carried out to determine the reduction potential E^0 for the Fe^{3+}/Fe^{2+} process of cyt *c* in water at infinite dilution (see Methods Section). This was done by measuring E^0 at decreasing ionic strength (I) from electrochemical experiments carried out at varying concentrations of sodium perchlorate (a typical cyclic voltammogram is reported in Figure 3). The intercept of the E^0 vs I plot yields the reduction potential at null I (see the section Electrochemical Measurements of the SI for further details). E^0 was found to linearly increase with decreasing ionic strength, as observed previously for several metalloproteins and different electrolytes.[46−48] Such a dependence can be confidently ascribed to the selective stabilization of one of the iron oxidation states by the ionic atmosphere and can be quantitatively described by the Debye−Hückel model. Nevertheless, effects on E^0 due to changes in the water availability induced by the decrease of ionic strength might also play a role and could induce a shift in E^0 for cyt *c* toward more positive values.[49,50] The experimental absolute reduction potential, which is needed for the comparison with the calculated value (see below), was obtained by adding a value of 4.420 V for the hydrogen semireaction[51] [which is that currently recommended

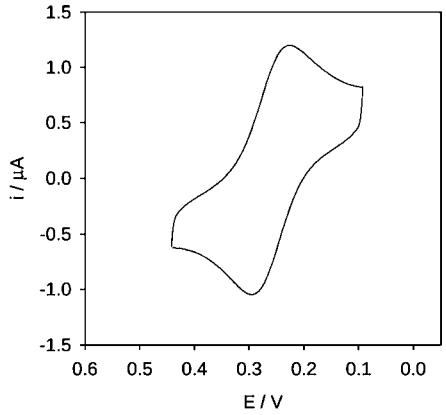

Figure 3. Cyclic voltammogram for wild-type recombinant *S. cerevisiae* iso-1-cytochrome *c* on a 4-mercaptopyridine-modified gold electrode in 2 mM phosphate buffer and 15 mM sodium perchlorate, pH 7. Scan rate = 0.05 V s^{-1}, T = 298 K.

by IUPAC for the standard hydrogen electrode (SHE)][52] to the reduction potential vs SHE extrapolated at infinite dilution (0.291 V vs SHE) yielding an absolute E^0 of 4.711 ± 0.002 V.

The absolute reduction potential E^0 was computed in water at zero ionic strength by averaging the values evaluated in the reduced and oxidized MD-simulation ensembles (see Methods Section). The time dependence of the difference between the perturbed ground-state electronic energy of the reduced and oxidized chemical states, $\Delta\varepsilon$, evaluated in the two ensembles and used in eq 7 to calculate E^0, is reported in Figure 4 for the

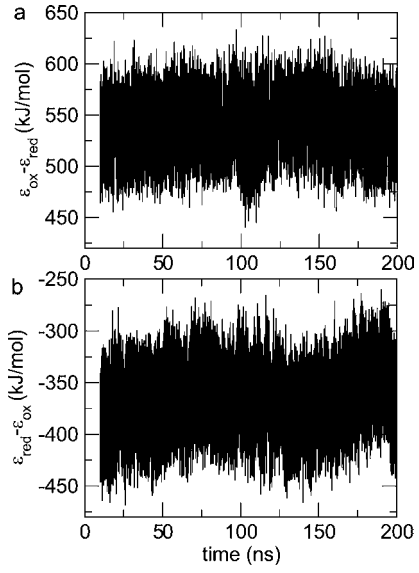

Figure 4. Time course of the difference between the perturbed ground-state electronic energy of the reduced and oxidized chemical states calculated from the reduced (a) and oxidized (b) cyt *c* simulation and used in eqs 4−7 to evaluate the redox thermodynamics. The first 10 ns of each simulation were removed for the thermodynamic analysis.

two ensembles. The computed E^0 values were 4.868 ± 0.016 and 4.573 ± 0.013 V in the reduced and oxidized ensembles, respectively, providing a mean E^0 value of 4.720 ± 0.014 V (details on the accuracy of the computed E^0 values are provided in the Theory Section of the SI).

The comparison between the calculated and experimental reduction potentials shows a very good agreement (see Figure 5). In fact, the calculated value is not significantly different from

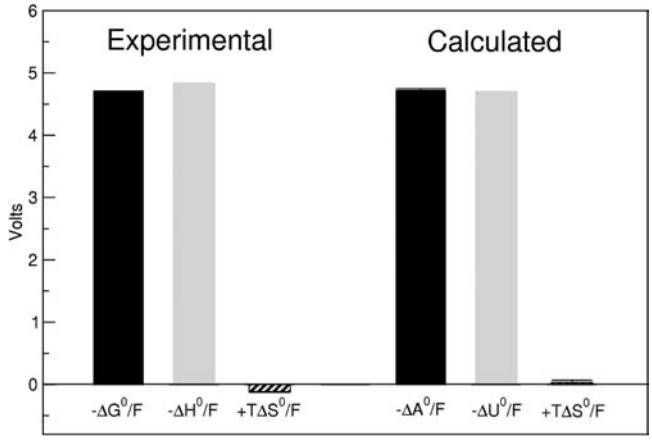

Figure 5. Calculated and experimental free energy (black), enthalpy/energy (gray), and entropy (striped) changes upon reduction at 298 K. Computed values: $-\Delta A^0/F$ = 4.720 ± 0.014 V, $-\Delta U^0/F$ = 4.687 ± 0.009 V, and $T\Delta S^0/F$ = 0.033 ± 0.016 V. Experimental values: $-\Delta G^0/F$ = 4.711 ± 0.002 V, $-\Delta H^0/F$ = 4.831 ± 0.009 V, and $T\Delta S^0/F$ = −0.120 ± 0.006 V. Errors reported throughout the article correspond to the standard error as obtained by considering four independent MD trajectories (two of the reduced cyt *c* and two of the oxidized cyt *c*) in the PMM calculations and five independent measurements in the experiments (details on the error calculations are given in the Evaluation of the Standard Errors Section of the SI).

the experimental one (4.720 ± 0.014 vs 4.711 ± 0.002 V, respectively). Such an agreement is remarkable if we consider that the theoretical approach used here does not rely on any adjustable, empirical parameter (see Theory Section in the SI). Clearly, the agreement also depends on the choice of the absolute potential for SHE to be used in the experimental determination of E^0, for which several different estimates are present in literature.[51−55] Nevertheless, computed and experimental values would still be very close (4.720 ± 0.014 vs 4.731 ± 0.002 V, respectively) if the IUPAC formerly recommended value of 4.440 V[53] was used instead of the currently recommended one. The energetic (enthalpic) and entropic contributions to the reduction potential can also be computed and compared to the experimental values. Partition of the total free energy change into these two contributions is an extremely powerful tool to investigate the molecular determinants of the reduction thermodynamics.[47,56] Calculated and measured energetic (enthalpic) and entropic contributions, shown in Figure 5, are also in good agreement. Clearly, the energetic (enthalpic) term prevails over the entropic one, favoring the reduction process.

The good agreement between experimental and computed results provides evidence of the reliability of the theoretical approach used for the calculation of the redox thermodynamics in protein. In particular, it indirectly shows the goodness of the simulations and thereby the robustness of the estimates of quantities which are not experimentally available (see next section). Moreover, given the rather small statistical errors on the computed quantities (≈10−20 mV), the PMM/MD approach may be potentially useful in carrying out predictive studies on different classes of cytochromes, which show variations in the reduction potential on the order of ≈100 mV.

dx.doi.org/10.1021/ja3030356 | J. Am. Chem. Soc. 2012, 134, 13670−13678

Effects of Cavity Opening on the Reduction Potential. The data reported in Figures 1 and 2 showed that the opening of the cavities allows water access inside the protein matrix. In particular, as cavities A and B face outer-propionate 6 and inner-propionate 7, respectively, their selective opening lead to an increase in the number of solvent molecules in the proximity of the carboxylate group of the corresponding propionate. To investigate possible effects on the reduction potential of changes in the hydration of each propionate, resulting from the opening of the corresponding cavity, the following procedure was used. For each cavity the PMM calculations were carried out on two subpopulations characterized by configurations with the propionate either dehydrated or hydrated, i.e., either 0 or 1−4 water molecules, respectively, are present within 0.35 nm of the carbon atom of the carboxylate group. The reduction potential E^0 is higher in the state in which the propionate is hydrated relative to the state in which the propionate is dehydrated, the change in E^0 being ΔE^0 = +44 ± 9 mV and +47 ± 8 mV for propionate 6 and 7, respectively (see Figure 6). Therefore, solvent access through

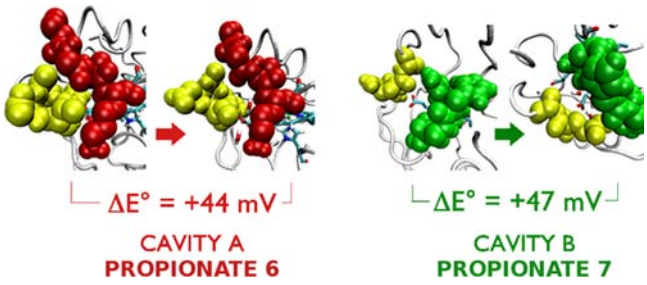

Figure 6. Changes in the reduction potential of cyt *c* upon solvent access to the heme crevice. Shift of the reduction potential, ΔE^0, between the conformational state in which one or more water molecules resides in the first hydration shell of propionate 6 (for cavity A, left) or 7 (for cavity B, right) and in the state in which the corresponding propionate is dehydrated. ΔE^0 is computed by averaging the ΔE^0 values evaluated in the reduced and oxidized ensembles. The standard errors on the ΔE^0 for cavity A and B are ±9 and ±8 mV, respectively.

the cavities in proximity of the heme carboxylate groups leads to a selective stabilization of the reduced heme, most probably because of a partial shielding of the negative charges on the propionates exerted by the water molecules.

This finding is only apparently in contrast with previous works[57,58] reporting on the decrease of the iron reduction potential as a consequence of the increase in exposure of the heme center to solvent. In fact, it is known that an increase in the solvent accessibility to the whole heme group leads to a stabilization of the oxidized form, as the more polar environment tends to favor Fe^{3+} over Fe^{2+}. Here, we are focusing on the effect of water on the negatively charged propionate groups only. Charge withdrawal from their carboxylic ends is known to lead to a stabilization of the reduced heme,[59−61] in agreement with our results. Moreover, the changes in the reduction potential that we observe as a function of water access to the heme propionates are consistent with experimental evidence concerning both the magnitude and sign of the observed variations. For example, the reduction potential for the N52I mutant of yeast cyt *c* is 58 mV more negative than that of the wild-type (WT) protein.[62,63] Comparison of the X-ray structures of the WT *c* and its N52I mutant reveals that, while the overall fold is not affected by the mutation, the so-called catalytic water molecule, located close to the outer propionate in the WT species, is missing in the structure of the mutant. Hence, the loss of a water molecule close to one of the propionates in the X-ray structure of the N52I mutant, resulting in an E^0 drop of −58 mV relative to the WT form, is in agreement with our findings. Finally, the conserved loop shielding the propionates from solvent was proposed to be one of the main determinants of the ET functionality of mithocondrial cytochromes *c*[64,65] and mutations of residues on this loop result in significant changes in E^0.

■ CONCLUSIONS

The present work investigates the dynamic protein−solvent interplay and its effects on functional properties, namely the reduction potential, in yeast cyt *c*. By means of a computational approach, tested against CV measurements, we show that cyt *c* switches between conformational states, accessible by thermal fluctuations, which are characterized by higher or lower levels of heme hydration, as a consequence of transient opening of solvent accessible cavities. Water molecules entering the protein matrix through these cavities can reach the heme propionates, causing a shift in the reduction potential E^0 of the Fe^{3+}/Fe^{2+} couple of about 50 mV toward more positive values.

Dynamic sampling of non-native states, as detected here, could have hardly been provided with the experimental tools currently available. This is due to the fact that the investigation of non-native, high-energy states are extremely challenging because most experimental techniques are dominated by signals associated with the predominantly populated native states. Nevertheless, our findings are supported by, and in some cases also help to explain, a number of experimental observations. The formation of solvent accessible channels is supported by hydrogen-exchange experiments[25] and investigation of the catalytic activity of cyt *c*,[27] while the magnitude and sign of the changes in E^0 upon hydration of the propionates are in agreement with structural and electrochemical data available for cyt *c* mutants.[62,63]

Our hypothesis is that these variations in the reduction potential might act as a mechanism of fine-tuning of E^0 for facilitating electron exchange events. For example, the kinetics of the ET process between cyt *c* and its physiological partners, that are known to be affected by the difference between their reduction potentials,[66] might be sped up by dynamical processes enabling transient, solvent-driven modulation of E^0, such as those observed here. One of the most thoroughly characterized interactions between cyt *c* and a physiological partner is that with cytochrome *c* peroxidase (CcP),[67] which is considered a paradigmatic case for biological ET. The structure of the complex between cyt *c* and CcP was obtained both by X-ray crystallography[68] and NMR.[69] Within the cells, cyt *c* transfers electrons to CcP when the two partners bind to form the short-time complex: transient shift of the reduction potential of cyt *c* toward more negative value would stabilize its oxidized form and therefore speed up the ET process. The comparison between the X-ray structures of cyt *c* bound to CcP with that of cyt *c* alone reveals a striking difference in the heme hydration: In the absence of the ET partner CcP, cyt *c* features two water molecules close to the inner propionate, while analysis of the structure of cyt *c* bound to CcP reveals that one of these two molecules is no longer present. How, and why, should a highly conserved water molecule leave its position close to propionate 7 upon binding to CcP? We believe that the

opening of a solvent accessible channel facing the inner propionate (as for example cavity B) could provide a way out for the water molecule. Moreover, according to our results, showing that an increase in the hydration of the propionates shifts the E^0 of the protein toward more positive values, it is conceivable to believe that the loss of this water molecule may serve as a tool to transiently adjust the reduction potential of cyt *c* toward more negative values, thus stabilizing its oxidized form and enhancing the ET rate. We therefore suggest that the water cavities presented here, the opening and closing mechanisms of which involve omega loops facing the heme propionates, could be a tool developed by cyt *c* for dynamic, controlled exposure of the heme to the solvent yielding a transient fine-tuning of its reduction potential.

METHODS

Protein Production and Electrochemical Measurements. WT recombinant untrimethylated *S. cerevisiae* iso-1-cyt *c* was expressed in *Escherichia coli* and purified following the procedure described elsewhere.[70] CV experiments were carried out at different scan rates (0.02−1 V s^{-1}) and temperatures (283−308 K) at pH = 7.0, using a cell for small volume samples (0.5 mL) under argon and a polycrystalline gold disk functionalized with 4-mercaptopyridine as the working electrode. The reduction potentials E^0 for cyt *c* were evaluated from the average of the anodic and cathodic peak potentials. E^0 was determined at different ionic strength values in order to extrapolate the value at null ionic strength, i.e., corresponding to infinitely diluted reactants and products, which is the reduction potential under consideration in the present work. More details concerning the electrochemical investigations can be found in the SI.

COMPUTATIONAL METHODS

MD simulations. The starting coordinates for the MD simulations of reduced and oxidized cyt *c* were taken from the crystal structures of the yeast iso-1-cyt *c* (pdb code 1YCC and 2YCC, respectively). The protein was put at the center of a dodecahedron box (volume = 107 nm^3) filled with 2942 single point charge (SPC)[71] water molecules and 4 chloride ions. A standard protocol was adopted for initiating the simulations. Following a mechanical solute optimization and subsequent solvent relaxation, the system was gradually heated from 50 to 298 K using short (20 ps) MD simulations. The trajectories were then propagated for 200 ns at 300 K in a NVT ensemble using an integration step of 2.0 fs. All bond lengths were constrained using the LINCS algorithm,[72] and the temperature was kept constant by the isokinetic temperature coupling.[73] Long-range electrostatics was computed by the particle mesh Ewald (PME) method[74] with a grid spacing of 0.12 nm combined with a fourth-order cubic interpolation. A real-space cutoff of 1.0 nm was used, and pair list was updated every five integration steps. The Gromos96 (53a6 version) force field parameters[75] were adopted for the protein and the heme in its reduced form. The atomic partial charges for the oxidized heme and the missing parameters describing axial and covalent links between the protein and the heme were parametrized using quantum chemical calculations (details are given in the Theory Section of the SI). For both the reduced and oxidized forms of cyt *c*, a second independent trajectory of 200 ns was performed to be used for evaluating the statistical errors on the thermodynamic properties. For the analysis the first 10 ns of each simulation were removed. All simulations were carried out using the Gromacs software.[76]

Quantum Chemical Calculations. In order to apply the PMM/MD procedure for the calculation of the redox properties (see below) it is first necessary to preselect the QC, i.e., the subportion of the simulated system to be treated explicitly at the electronic level. In the present case the atoms of the prosthetic group and of the side chains of the axial ligands, i.e., one histidine and one methionine, were selected as QC (details on the choice of the QC are given in the Theory Section of the SI).

For obtaining the unperturbed ground-state energies and related properties to be used in the PMM procedure, quantum chemical calculations were performed on the isolated QC for both redox states of the QC, i.e., with the iron(II) and iron(III), at the time-dependent density functional theory (TD-DFT) level with Becke's three parameters exchange and Lee, Yang, and Parr correlation functionals (B3LYP). The atomic basis sets were as follows: (i) for the iron atom we used the LANL2DZ effective core potential for the inner electrons and a double Gaussian basis set of (5S,5P,5D)/[3S,3P,2D] quality for the valence electrons;[77] (ii) for the hydrogen, carbon, nitrogen, oxygen, and sulfur atoms we used a standard 6-31+G(d)[78] Gaussian basis set. The first 12 unperturbed excited electronic (vertical) states were obtained on the ground-state geometry using TD-DFT calculations. Although in general this level of theory might not provide a fully correct description of electronic excited states, in the case of the heme group it has already proved to represent a good compromise between computational costs and chemical accuracy.[79] All quantum chemical calculations were carried out using the Gaussian03 package.[80]

Structural Analysis. The program CASTp[81] was used to identify the presence of cavities connecting the heme pocket to the solvent and the residues defining the given cavity, in the MD simulations. In particular, 200 structures extracted every 1 ns along the 200 ns long simulation of the reduced cyt *c* were utilized. Analysis of the oxidized cyt *c* simulation revealed a similar pattern of cavities as in the reduced ensemble. The distances between the C_α atoms of residues 50 and 77 and the C_α atoms of residues 31 and 43 were taken to define if cavity A and B, respectively, are in a closed (distance < cutoff) or open (distance ≥ cutoff) conformation. The cutoff values (0.62 and 0.65 nm for cavity A and B, respectively) were chosen from the probability density profile plotted as a function of the C_α−C_α distance and by taking as the cutoff value the distance at which the profile exhibits a local minimum between the two main peaks. Each cavity was approximated, frame by frame, with the ellipsoid that fits best the atoms defining the cavity, i.e., the C_α atoms of the residues identified by the program CASTp and the C atom of the carboxylate group of the propionate facing the cavity, in order to determine the number of water molecules residing inside; a water molecule is considered to occupy the cavity if its center of mass lies within the ellipsoid. The PCA, also called essential dynamics analysis,[41,42] was applied to all atoms of a given cavity, using all structures generated in the reduced and oxidized cyt *c* trajectories, to analyze the motions involved in the opening/closing processes. Here, for each cavity the first eigenvector, i.e., the one with the highest eigenvalue, was found to accurately describe opening/closing motions as it clearly involves backbone movements, rather than single side chain displacements. The first eigenvector captures 27% and 43% of the motion for cavities A and B, respectively.

Redox Potentials. In the present paper we consider cyt *c* redox thermodynamics at 298 K at infinite dilution conditions in both the experimental and theoretical/computational evaluations. Experimentally, the (Gibbs) free energy change (ΔG^0) associated to the isobaric $Fe^{+3} + e^- \rightarrow Fe^{+2}$ semireaction was evaluated as

$$\Delta G^0 = \Delta G^0_{ox\rightarrow red} = -FE^0 \quad (1)$$

In the above equation E^0 is the reduction potential of the given semireaction, i.e., a value of 4.420 V for the hydrogen semireaction[51] was added to the reduction potential vs SHE measured in the experiments (0.291 V vs SHE). The entropic and enthalpic contributions to ΔG^0 were determined from variable-temperature CV experiments (details are given in the Electrochemical Measurements Section of the SI). The entropy for reduction of the oxidized protein (ΔS^0) was determined from the slope of the plot of E^0 vs temperature, which turned out to be linear under the assumption that ΔS^0 is constant over the limited temperature range investigated:

$$\Delta S^0 = \Delta S^0_{ox\rightarrow red} = nF(\partial E^0/\partial T) \quad (2)$$

The ΔH^0 value was then obtained as

dx.doi.org/10.1021/ja3030356 | J. Am. Chem. Soc. 2012, 134, 13670−13678

$$\Delta H^0 = \Delta H^0_{ox\rightarrow red} = \Delta G^0 + T\Delta S^0 \quad (3)$$

In the PMM/MD calculations[19−22] the thermodynamic changes were evaluated at fixed volume rather than at fixed pressure. While the Gibbs and Helmholtz free energy changes upon reduction coincide when evaluated at fixed pressure or volume, respectively (i.e., providing the chemical potential variation), the computed energy/entropy changes are fully equivalent to the experimental enthalpy/entropy changes only if the partial molar volume of the protein does not change significantly upon reduction/oxidation. Given that cyt *c* exhibits, as expected, a tiny volume change during electron transfer,[82] we expect differences between the experimental enthalpy/entropy and the computed internal energy/entropy due to partial molar volume changes to be negligible, i.e., within the noise.

The (Helmholtz) free energy (ΔA^0), internal energy (ΔU^0), and entropy (ΔS^0) changes upon reduction were calculated using the following equations (ΔA^0 is related to the reduction potential via $E^0 = -\Delta A^0/F$) (details are given in the Theory Section of the SI):

$$\Delta A^0 = \Delta A^0_{ox\rightarrow red} \cong -k_B T \ln\langle e^{-\beta\Delta\varepsilon_{ox\rightarrow red}}\rangle_{ox} = k_B T \ln\langle e^{\beta\Delta\varepsilon_{ox\rightarrow red}}\rangle_{red} \quad (4)$$

$$\Delta U^0 = \Delta U^0_{ox\rightarrow red} \cong \frac{1}{2}(\langle\Delta\varepsilon_{ox\rightarrow red}\rangle_{ox} + \langle\Delta\varepsilon_{ox\rightarrow red}\rangle_{red}) \quad (5)$$

$$\Delta S^0 = \Delta S^0_{ox\rightarrow red} = \frac{\Delta U^0 - \Delta A^0}{T} \quad (6)$$

In the above equations $\Delta\varepsilon_{ox\rightarrow red} = \varepsilon_{red} - \varepsilon_{ox}$, with ε_{red} and ε_{ox} representing the perturbed ground-state electronic energy of the reduced (red) and oxidized (ox) chemical states, respectively. At each MD frame, ε_{red} and ε_{ox} are evaluated via the PMM approach, i.e., by diagonalizing at each MD frame the perturbed Hamiltonian matrices of the reduced and oxidized QC, respectively (details of the PMM procedure are given in the Theory Section of the SI), and the averaging is performed in the reduced or oxidized ensemble as indicated by the angle brackets subscript. Although eq 4 is based on in principle an exact relation, given the sampling problems of finite-time simulations, the best estimate of the reduction free energy is obtained by averaging the values provided by the reduced and oxidized ensembles:[13]

$$\Delta A^0_{ox\rightarrow red} \cong \frac{-k_B T \ln\langle e^{-\beta\Delta\varepsilon_{ox\rightarrow red}}\rangle_{ox} + k_B T \ln\langle e^{\beta\Delta\varepsilon_{ox\rightarrow red}}\rangle_{red}}{2} \quad (7)$$

Concerning the internal energy and entropy changes provided by eqs 5 and 6, these are only approximations based on a relevant assumption (see the Theory Section in the SI) hence implying that, differently from the ΔA^0 estimate, ΔU^0 and ΔS^0 may be affected by significant systematic errors.

■ ASSOCIATED CONTENT

Supporting Information

Details on the theory, simulations, and experiments performed. This material is available free of charge via the Internet at http://pubs.acs.org.

■ AUTHOR INFORMATION

Corresponding Author

daidone@caspur.it

Notes

The authors declare no competing financial interest.

■ ACKNOWLEDGMENTS

The work was supported by CASPUR HPC grant 2011 "Theoretical study of electron-transfer reactions in complex atomic-molecular systems". I.D., A.A. and M.A. acknowledge CASPUR for the use of Gaussian. S.C. acknowledges funding from IIT Platform Computational through the Seed project MOPROSURF.

■ REFERENCES

(1) Lange, O. F.; Lakomek, N.; Fares, C.; Schroeder, G. F.; Walter, K. F. A.; Becker, S.; Meiler, J.; Grubmueller, H.; Griesinger, C.; de Groot, B. L. *Science* **2008**, *320*, 1471−1475.

(2) Skourtis, S. S.; Waldeck, D. H.; Beratan, D. N. *Annu. Rev. Phys. Chem.* **2010**, *61*, 461−485.

(3) Skourtis, S. S.; Balabin, I. A.; Kawatsu, T.; Beratan, D. N. *Proc. Natl. Acad. Sci. U.S.A.* **2005**, *102*, 3552−3557.

(4) Hoffman, B. M.; Celis, L. M.; Cull, D. A.; Patel, A. D.; Seifert, J. L.; Wheeler, K. E.; Wang, J.; Yao, J.; Kurnikov, I. V.; Nocek, J. M. *Proc. Natl. Acad. Sci. U.S.A.* **2005**, *102*, 3564−3569.

(5) Goodsell, D. S. *The machinery of life*; Springer-Verlag: New York, 2009.

(6) Sagle, L. B.; Zimmermann, J.; Matsuda, S.; Dawson, P. E.; Romesberg, F. E. *J. Am. Chem. Soc.* **2006**, *128*, 7909−7915.

(7) Krishna, M. M. G.; Lin, Y.; Rumbley, J.; Englander, W. S. *J. Mol. Biol.* **2003**, *331*, 29−36.

(8) Henzler-Wildman, K.; Kern, D. *Nature* **2007**, *450*, 964−972.

(9) Banci, L. *Curr. Opin. Chem. Biol.* **2003**, *7*, 143−149.

(10) Wand, A. J. *Nat. Struct. Biol.* **2001**, *8*, 926−931.

(11) Benkovic, S.; Hammes-Schiffer, S. *Science* **2003**, *301*, 1196−1202.

(12) Stock, A. *Nature* **1999**, *400*, 221−222.

(13) Muegge, I.; Qi, P. X.; Wand, A. J.; Chu, Z. T.; Warshel, A. *J. Phys. Chem. B* **1997**, *101*, 825−836.

(14) Pu, J.; Gao, J.; Truhlar, D. *Chem. Rev.* **2006**, *106*, 3140−3169.

(15) Cascella, M.; Magistrato, A.; Tavernelli, I.; Carloni, P.; Rothlisberger, U. *Proc. Natl. Acad. Sci. U.S.A.* **2006**, *103*, 19641−19646.

(16) Dal Peraro, M.; Ruggerone, P.; Raugel, S.; Gervasio, F. L.; Carloni, P. *Curr. Opin. Struc. Biol.* **2007**, *17*, 149−156.

(17) Tipmanee, V.; Oberhofer, H.; Park, M.; Kim, K. S.; Blumberger, J. *J. Am. Chem. Soc.* **2010**, *132*, 17032−17040.

(18) van den Bosch, M.; Swart, M.; Snijders, J. G.; Berendsen, H. J. C.; Mark, A. E.; Oostenbrink, C.; van Gunsteren, W.; Canters, G. W. *ChemBioChem* **2005**, *6*, 738−746.

(19) Aschi, M.; Spezia, R.; Di Nola, A.; Amadei, A. *Chem. Phys. Lett.* **2001**, *344*, 374−380.

(20) Amadei, A.; D'Alessandro, M.; Aschi, M. *J. Phys. Chem. B* **2004**, *108*, 16250−16254.

(21) Zazza, C.; Amadei, A.; Palma, A.; Sanna, N.; Tatoli, S.; Aschi, M. *J. Phys. Chem. B* **2008**, *112*, 3184−3192.

(22) Amadei, A.; Daidone, I.; Di Nola, A.; Aschi, M. *Curr. Opin. Struc. Biol.* **2010**, *20*, 155−161.

(23) Gao, J.; Truhlar, D. G. *Annu. Rev. Phys. Chem.* **2002**, *53*, 467−505.

(24) Meier, K.; Thiel, W.; van Gunsteren, W. F. *J. Comput. Chem.* **2012**, *33*, 363−378.

(25) Maity, H.; Maity, M.; Krishna, M.; Mayne, L.; Englander, S. *Proc. Natl. Acad. Sci. U.S.A.* **2003**, *102*, 4741−4746.

(26) Goodsell, D. S. *The Oncologist* **2004**, *9*, 226−227.

(27) Kagan, V. E.; A.Tyurin, V.; Jiang, J.; Tyurina, Y. Y.; Ritov, V. B.; Amoscato, A. A.; Osipov, A. N.; Belikova, N. A.; Kapralov, A. A.; Kini, V.; Vlasova, I. I.; Zhao, Q.; Zou, M.; Di, P.; Svistunenko, D. A.; Kurnikov, I. V.; Borisenko, G. G. *Nat. Chem. Biol.* **2005**, *1*, 223−232.

(28) Belikova, N. A.; Vladimirov, Y. A.; Osipov, A. N.; Karpalov, A. A.; Tyurin, V. A.; Potapovich, M. V.; Basova, L. V.; Peterson, J.; Kurnikov, I. V.; Kagan, V. E. *Biochemistry* **2006**, *450*, 964−972.

(29) Banci, L.; Gori-Savellini, G.; Turano, P. *Eur. J. Biochem.* **1997**, *249*, 716−723.

(30) Lange, C.; Hunte, C. *Proc. Natl. Acad. Sci. U.S.A.* **2002**, *99*, 2800−2805.

(31) Solmaz, S. R. N.; Hunte, C. *J. Biol. Chem.* **2008**, *283*, 17542−17549.

(32) Lin, J.; Balabin, I.; Beratan, D. *Science* **2005**, *310*, 1311−1313.

(33) de la Lande, A.; Babcock, N. S.; Rezac, J.; Sanders, B. C.; Salahub, D. R. *Proc. Natl. Acad. Sci. U.S.A.* **2010**, *107*, 11799−11804.

(34) Olsson, M. H. M.; Hong, G.; Warshel, A. *J. Am. Chem. Soc.* **2003**, *125*, 5025−5039.
(35) Louie, G. V.; Brayer, G. D. *J. Mol. Biol.* **1990**, *214*, 527−555.
(36) Humprey, W.; Dalke, A.; Schulten, K. *J. Mol. Graphics* **1996**, *14*, 33−38.
(37) Karpishin, T. V.; Grinstaff, M. W.; Komar-Panicucci, S.; McLendon, G.; Gray, H. B. *Structure* **1994**, *2*, 415−422.
(38) Langen, R.; Colon, J. L.; Casimiro, D. R.; Karpishin, T. V.; Winkler, J. R.; Gray, H. B. *J. Biol. Inorg. Chem.* **1996**, *1*, 221−225.
(39) Beratan, D. N.; Onuchic, J.; Bowler, J. N. B. B. E.; Gray, H. *J. Am. Chem. Soc.* **1990**, *112*, 7915−1921.
(40) Bortolotti, C. A.; Borsari, M.; Sola, M.; Chertkova, R.; Dolgickh, D.; Kotlyar, A.; Facci, P. *J. Phys. Chem. C* **2007**, *111*, 12100−12105.
(41) Garca, A. *Phys. Rev. Lett.* **1992**, *66*, 2696−2699.
(42) Amadei, A.; Linssen, A. B. M.; Berendsen, H. J. C. *Proteins: Struct. Funct. Genet.* **1993**, *17*, 412−425.
(43) Wang, L.; Kallenbach, N. R. *Protein Sci.* **1998**, *7*, 260−264.
(44) Spoalore, B.; Bermejo, R.; Zambonin, M.; Fontana, A. *Biochemistry* **2001**, *40*, 9460−9468.
(45) Assfalg, M.; Bertini, I.; Del Conte, R.; Turano, P. *Biochemistry* **2007**, *46*, 6232−6238.
(46) Gopal, D.; Wilson, G. S.; Earl, R. A.; Cusanovich, M. A. *J. Biol. Chem.* **1988**, *263*, 11652−11656.
(47) Battistuzzi, G.; Borsari, M.; Loschi, L.; Sola, M. *J. Biol. Inorg. Chem.* **1999**, *4*, 601−607.
(48) Moore, G. R.; Pettigrew, G. W. *Cytochromes c: evolutionary, structural and physicochemical aspects*; Springer: New York, 1990.
(49) Bilanicova, D.; Salis, A.; Ninham, B.; Monduzzi, M. *J. Phys. Chem. B* **2008**, *112*, 12066−12072.
(50) Parsegian, V. A.; Rand, R. P.; Rau, D. C. *Proc. Natl. Acad. Sci. U.S.A.* **2000**, *97*, 3987−3992.
(51) Fawcett, W. R. *Langmuir* **2008**, *24*, 9868−9875.
(52) Isse, A. A.; Gennaro, A. *J. Phys. Chem. B* **2010**, *114*, 7894−7899.
(53) Trasatti, S. *Pure Appl. Chem.* **1986**, *58*, 955−966.
(54) C. P. Kelly, C. J. C.; Thrular, D. G. *J. Phys. Chem. B* **2006**, *110*, 16066−16081.
(55) C. P. Kelly, C. J. C.; Thrular, D. G. *J. Phys. Chem. B* **2007**, *111*, 408−422.
(56) Battistuzzi, G.; Borsari, M.; Cowan, J. A.; Ranieri, A.; Sola, M. *J. Am. Chem. Soc.* **2002**, *124*, 5315−5324.
(57) Fantuzzi, A.; Sadeghi, S.; Valetti, F.; Rossi, G. L.; Gilardi, G. *Biochemistry* **2002**, *41*, 8718−8724.
(58) Tezcan, F. A.; Winkler, J. R.; Gray, H. B. *J. Am. Chem. Soc.* **1998**, *120*, 13383−13388.
(59) Dolla, A.; Blanchard, L.; Guerlesquin, F.; Bruschi, M. *Biochimie* **1994**, *76*, 471−479.
(60) Unno, M.; Shimada, H.; Toba, Y.; Makino, R.; Ishimura, Y. *J. Biol. Chem.* **1996**, *271*, 17869−17874.
(61) Moore, G. R.; Williams, R. J. P.; Peterson, J.; Thomson, A. J.; Mathews, F. S. *Biochim. Biophys. Acta* **1985**, *829*, 83−96.
(62) Lett, C. M.; Guillemette, J. G. *Biochem. J.* **2002**, *362*, 261−267.
(63) Berghuis, A. M.; Guillemette, J. G.; Smith, M.; Brayer, G. D. *J. Mol. Biol.* **1994**, *235*, 1326−1341.
(64) Berry, E.; Huang, L.; Saechao, L.; Pon, N.; Valkova-Valchanova, M; Daldal, F. *Photosynth. Res.* **2004**, *81*, 251−275.
(65) Osyczka, A.; Dutton, P.; Moser, C.; Darrouzet, E.; Daldal, F. *Biochemistry* **2001**, *40*, 14547−14556.
(66) Bendall, D. S. *Protein Electron Transfer*; BIOS Scientific Publishers Ltd: Oxford, U.K., 1996.
(67) Mathews, F. S.; Mauk, A. G.; Moore, G. R. In *Protein-Protein Recognition*; Kleanthous, C., Ed.; Oxford Univ Press, New York, 2006; pp 60−101.
(68) Pelletier, H.; Kraut, J. *Science* **1992**, *258*, 1748−1755.
(69) Volkov, A.; Worral, J.; Holtzmann, E.; Ubbink, M. *Proc. Natl. Acad. Sci. U.S.A.* **2006**, *103*, 18945−18950.
(70) Battistuzzi, G.; Borsari, M.; Bortolotti, C. A.; Rocco, G. D.; Ranieri, A.; Sola, M. *J. Phys. Chem. B* **2007**, *111*, 10281−10287.
(71) Berendsen, H. J. C.; Grigera, J. R.; Straatsma, T. P. *J. Phys. Chem.* **1987**, *91*, 6269−6271.
(72) Hess, B.; Bekker, H.; Berendsen, H. J. C.; Fraaije, J. G. E. M. *J. Comput. Chem.* **1997**, *18*, 1463−1472.
(73) Brown, D.; Clarke, J. H. R. *Mol. Phys.* **1984**, *51*, 1243−1252.
(74) Darden, T.; York, D.; Pedersen, L. *J. Chem. Phys.* **1993**, *98*, 10089−10092.
(75) van Gunsteren, W. F.; Billeter, S. R.; Eising, A. A.; Hünenberger, P. H.; Krüger, P.; Mark, A. E.; Scott, W. R. P.; Tironi, I. G. *Biomolecular Simulation: The GROMOS96 Manual and User Guide*; Verlag der Fachvereine Hochschulverlag AG an der ETH Zurich: Zurich, Switzerland, 1996.
(76) Berendsen, H. J. C.; van der Spoel, D.; van Drunen, R. *Comput. Phys. Commun.* **1995**, *95*, 43−56.
(77) Hay, P. J.; Wadt, W. R. *J. Chem. Phys.* **1985**, *82*, 299−310.
(78) Krishnan, R.; Binkley, J. S.; Seeger, R.; Pople, J. A. *J. Chem. Phys.* **1980**, *72*, 650−654.
(79) Aschi, M.; Zazza, C.; Spezia, R.; Bossa, C.; Di Nola, A.; Paci, M.; Amadei, A. *J. Comput. Chem.* **2004**, *25*, 974−984.
(80) Frisch, M. J. et al. *Gaussian 03, Revision C.02*; Gaussian, Inc.: Wallingford, CT, 2004.
(81) Dundas, J.; Ouyang, Z.; Tseng, J.; Binkowski, A.; Turpaz, Y.; Liang, J. *Nucleic Acids Res.* **2006**, *34*, W116−W118.
(82) Sun, J.; Wishart, J. F.; van Eldik, R.; Shalders, R. D.; Swaddle, T. W. *J. Am. Chem. Soc.* **1995**, *117*, 2600−2605.